

Geophysical Research Letters®

RESEARCH LETTER

10.1029/2022GL098211

Key Points:

- The fiber-optic nerve system with weak-reflection fiber Bragg gratings produces multi-physical spatiotemporal profiles at high resolutions
- Thermo-hydro-mechanical responses at the slip surface uncover subsurface-scale landslide kinematics, hydrological transport and retention
- Short-duration high-intensity rainfalls promote landslide dynamics relative to uniform-intensity rainfalls of similar amount and duration

Supporting Information:

Supporting Information may be found in the online version of this article.

Correspondence to:



H.-H. Zhu,
zhz@nju.edu.cn

Citation:

Ye, X., Zhu, H.-H., Wang, J., Zhang, Q., Shi, B., Schenato, L., & Pasuto, A. (2022). Subsurface multi-physical monitoring of a reservoir landslide with the fiber-optic nerve system. *Geophysical Research Letters*, 49, e2022GL098211. <https://doi.org/10.1029/2022GL098211>

Received 23 FEB 2022
Accepted 26 MAY 2022

Subsurface Multi-Physical Monitoring of a Reservoir Landslide With the Fiber-Optic Nerve System

Xiao Ye¹, Hong-Hu Zhu¹ , Jia Wang¹, Qin Zhang², Bin Shi¹ , Luca Schenato³, and Alessandro Pasuto³

¹School of Earth Sciences and Engineering, Nanjing University, Nanjing, China, ²College of Geology Engineering and Geomatics, Chang'an University, Xi'an, China, ³National Research Council-Research Institute for Geo-Hydrological Protection (CNR-IRPI), Padova, Italy

Abstract Reservoir landslides are typical geohazards with sophisticated thermo-hydro-mechanical interactions. However, direct observations of subsurface multi-physical processes in bank slopes remain rare. Herein we present the design, implementation and evaluation of an innovative fiber-optic nerve system based on weak-reflection fiber Bragg grating to monitor a giant landslide located in the Three Gorges Reservoir region, China. The system is capable of measuring and imaging spatiotemporal distributions of temperature, moisture and strain along boreholes in near real-time. Such visual profiles offer unique insights into the subsurface thermo-hydro-mechanical link between external conditions and geotechnical deformation, making it possible to decipher the substantial trigger of accelerated movements. Multi-physical responses at depths of interest also enable us to better understand the evolution mechanism of reservoir landslides. Fiber-optic nerve sensing can synergize with remote sensing and surface-based technologies to build a space-sky-ground-subsurface integrated monitoring system for landslides.

Plain Language Summary Field monitoring of multi-physical processes of reservoir landslides in the context of extreme weather events has remained challenging. Here we present the design, implementation and evaluation of a novel fiber-optic nerve system (FONS) and the results and interpretation of recent FONS monitoring at the Outang landslide in the Three Gorges Reservoir region, China. The spatiotemporal profiles of subsurface temperature, moisture and strain are obtained, which enable us to understand the subsurface thermo-hydro-mechanical interactions. The deep-seated slip surface has been successfully identified, together with a shallower one newly generated in the rear section of the landslide. We further verify that precipitation was the substantial trigger of accelerated deformation in the rear slope, and argue that short-duration high-intensity extreme rainfall was most likely to drive an abrupt movement. The monitoring system allows us to investigate the characteristics and mechanism of specific deformation acceleration events from daily to annual time series and relate the thermo-hydro-mechanical behaviors of sliding masses to creeping motion and progressive failure.

1. Introduction

The reservoir landslide is a ubiquitous geohazard that features thermo-hydro-mechanical interactions. Once a catastrophic collapse occurs, it will represent a serious threat to the safe operation of dams as well as to other engineering structures and people living along reservoir banks (Lacroix et al., 2020; Yin et al., 2016). In the context of extreme climate, there is growing concern that the changes in temperature, precipitation, and floods can adversely affect the operation of infrastructure networks in the reservoir area (Aghakouchak et al., 2018; Wasko et al., 2015). Consequently, the past decade has witnessed an increasing frequency of disastrous landslides with cascading impacts (Brovkin et al., 2021; Cook et al., 2021; Liu et al., 2020). Taking China's Three Gorges Reservoir (TGR) as an example, the cumulative precipitation from May–July 2020 exceeded 500 mm, which made 2020 the most severe flood year since 1998, triggering a large number of landslide movements and collapses within the area (Wei et al., 2020). Accordingly, various cutting-edge monitoring technologies for landslides are expected to help inform with this severe situation.

Remote sensing and ground-based observation techniques can characterize landslide deformation at different spatial scales and frequencies but only apply to surface displacements or velocities (Biggs & Wright, 2020; Cenni et al., 2021; Hu et al., 2018; Strozzi et al., 2010). Instead, borehole-based geotechnical instrumentation may be a useful approach to understand how a landslide develops and evolves. Fiber Bragg grating (FBG), a popular fiber optic sensing technology, enables borehole monitoring of strain, temperature and groundwater-related data (Zhu

et al., 2017). However, the arrangement of several discrete FBG sensors (i.e., usually less than 10) can only obtain discrete subsurface multi-physical information, making it difficult to interpret as a whole (Sun et al., 2014). Distributed fiber optic sensing (DFOS) can acquire abundant data on temperature, strain and vibration along an optical fiber. Nevertheless, establishing an automatic real-time monitoring system is challenging due to the limitations in spatial resolution and scanning rates (Shi et al., 2021; Zeni et al., 2015). Consequently, weak-reflection fiber Bragg grating (WFBG), combining the advantages of FBG with DFOS (Table S1 in Supporting Information S1), provides a high spatial resolution up to several centimeters and acts as a densely spaced sensing array (Li & Zhang, 2018). However, very limited literature on landslide multi-physical monitoring using WFBG has been reported.

This paper presents the design, implementation, and performance evaluation of a novel fiber-optic nerve system (FONS) to capture subsurface thermo-hydro-mechanical behavior, which has been established on the Outang landslide in the TGR region, China. With its large volume of ~ 90 million m^3 and perennial motions at ~ 100 – 500 mm per year, this slow-moving landslide has a long history of conventional in-situ monitoring and represents a desirable natural laboratory to better understand multi-physical interactions of such landslides. Herein, we report the monitoring results within the whole flood season and produce the spatiotemporal profiles of temperature, moisture and strain along a vertical borehole in the landslide. Such a critical dataset also allows us to decipher the main driver of accelerated movements through a joint analysis of in-situ displacements and hydrometeorological records. This work provides improved insights into the long-term subsurface evolution mechanisms and dynamics of reservoir landslides.

2. Methodology

2.1. WFBG-Based Fiber-Optic Nerve System

In recent years, the DFOS-based temperature profiling method has shed new light on the investigation of subsurface hydrogeological characteristics (Bakker et al., 2015; Read et al., 2013; Sayde et al., 2010). This paper proposes a novel FONS system based on WFBG technology for acquiring subsurface multi-physical information of reservoir landslides, consisting of in-situ monitoring, wireless data transmission, and a data server (Figure 1a). Three types of tailored WFBG-based fiber optic cables, acting as underground nerves, are designed to be installed in a borehole to dynamically sense the soil temperature, moisture content, and strain profiles. All the WFBGs are connected in series with a 1 m spacing. All the measurement- and transmission-relevant equipment is placed in a cabinet at the slope surface, allowing for remote real-time monitoring of subsurface thermo-hydro-mechanical information (Text S1).

The specially manufactured fiber optic cables were developed by Nanjing University and the technical details can be found in Figure S1, Table S2 and S3 in Supporting Information S1. Note that these sensing cables have been calibrated in the laboratory before field instrumentation (Text S2 in Supporting Information S1). Typical calibration results are shown in Figures S2 and S3 in Supporting Information S1.

For the temperature and moisture sensing cables, the bare fiber is installed in a loose tube to eliminate the influence of strain on the cable. For the strain sensing cable, temperature compensation is conducted to obtain accurate strain measurements. As soil moisture content is closely related to macroscopic thermophysical characteristics, the actively heated WFBG (AH-WFBG) technique is utilized to monitor soil moisture conditions (Cao et al., 2018). The empirical relationship between the soil moisture content and temperature response of the soil-embedded sensing cable to heating can be described as (Cao et al., 2015):

$$\theta = k\Delta T + b \quad (1)$$

where θ is the volumetric moisture content; ΔT is the temperature increment due to active heating; k and b are two constants that can be determined through several sets of calibration tests.

2.2. Principle of WFBG

As illustrated in Figure 1b, WFBG is a particular type of fiber grating with ultra-weak reflectivity, which allows near-distributed temperature and strain sensing. When broadband incident light reaches a WFBG, a small part of the signal light close to the central wavelength of the WFBG is reflected, and the remaining light travels forward to the

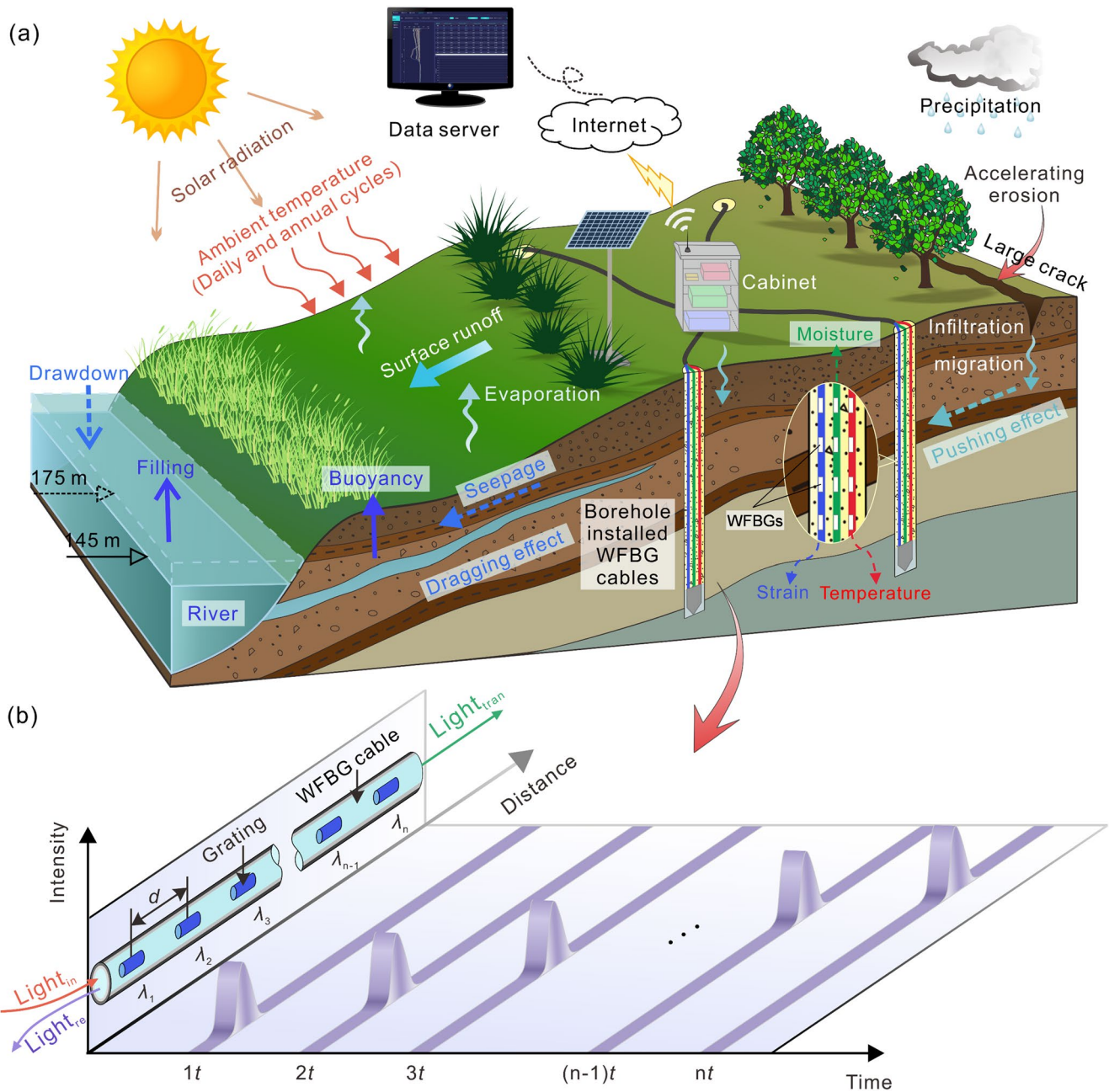


Figure 1. Fiber-optic nerve system for characterizing thermo-hydro-mechanical behavior of reservoir landslides. (a) Conceptual map of the fiber-optic nerve system (FONS) and illustration of the evolution mechanism of reservoir landslides under different external conditions. The solid/dashed blue arrow indicates the filling/dropping of the reservoir water level (RWL), inducing the buoyancy and seepage force in the leading part of the slide. The dashed curved aquamarine arrows represent surface evaporation under daily and annual atmospheric temperature cycles, as well as rainfall infiltration into layered soils and even migration to slip surfaces. (b) Principle of weak-reflection fiber Bragg grating (WFBG) sensing.

next WFBG. The shift in central wavelength of the reflected light maintains a linear relationship with the temperature or strain change (Kersey et al., 1997). Unlike the wavelength-division multiplexing technique of conventional FBG, the WFBG utilizes time-division multiplexing for signal transmission. Hence, the quantity of multiplexed gratings is no longer limited by the bandwidth of the light source. Intriguingly, thousands of WFBGs with the same central wavelength ($\lambda_1 = \lambda_2 = \dots = \lambda_n$) can be multiplexed in an optical fiber, forming a densely spaced temperature or strain sensing array. Each grating in the array can be localized using the optical time-domain reflectometer technology owing to the time difference of reflective gratings at different positions (Liu et al., 2021).

3. Investigated Landslide

The Outang landslide is located on the right bank of the Yangtze River in Fengjie, Chongqing, China (Figure S4 in Supporting Information S1). As outlined in Figure 2, the landslide covers a total area of 1.77 million m² and a volume of approximately 90 million m³, which has been of great concern as one of the largest landslides in the TGR area. The landslide can be divided into three subzones (Text S3 in Supporting Information S1). The elevation of the front edge is 90–102 m.a.s.l., which is lower than the 145–175 m reservoir water level (RWL) in operation. Thus the landslide toe is completely submerged. Below the Quaternary soils, with a thickness of 10–18 m, is a fractured quartz sandstone layer formed during the Jurassic period, with a thickness of 25–90 m. Tens of thin and weak layers (i.e., 0.3–1 m thick) composed of dark gray silt clay with gravel or gray-black carbonaceous shale are intercalated in this formation, which has been identified as the possible sliding surfaces of the landslide (Wang et al., 2021).

This landslide has a long history of conventional in-situ monitoring (Figure 2a). The average surface velocities recorded by GNSS from 2011 to 2020 reveal the spatial distribution over the landslide (Text S4 in Supporting Information S1). Time-variant cumulative displacements are characterized by a cyclic alternation of short-duration fast-movement and long-duration quasi-static behavior. Despite larger values of cumulative displacement in the landslide toe, the velocities in the head part are more conspicuous than those in the toe, implying that the rear slope is likely to be the most active subzone in the coming years (Figure S5 in Supporting Information S1). Surface displacements exhibit an ongoing step-like growth.

In this framework, the fast-moving rear part of the landslide has been preferably selected as a survey site (109°21'21.36"E, 30°57'23.68"N, ~462 m) to deploy the FONS system we developed. As mentioned above, three WFBG sensing cables have been clustered into a bundle and arranged in a vertical borehole with a diameter of 110 mm, crossing the sliding mass for capturing soil temperature, moisture, and strain (Figure S6 in Supporting Information S1). After the sensing cables were placed, borehole backfilling was performed with a sand-centered mixture to assure satisfactory coupling of the sensing cables to the surrounding geomaterials (Text S5 in Supporting Information S1; Zhang, Shi, et al., 2018; Shi et al., 2019). Detailed data acquisition frequency and heating control for the moisture measurement can be found in Text S6 in Supporting Information S1. Thermal effects of the AH-WFBG testing on the temperature, moisture and strain measurements can be found in Figure S7 and Text S7 in Supporting Information S1.

4. Spatiotemporal Distribution of Subsurface Multi-Physical Information

The subsurface temperature profile is characterized by a variable temperature zone within a depth of ~7 m and a nearly constant temperature zone below the depth (Figures 3a and S8). The time-varying surface temperature agrees well with the atmospheric temperature records. The temperature response in the variable temperate zone was much more sensitive than that in deeper soils. This was attributed to the influence of solar radiation and surface evaporation/infiltration at shallower depths (Freifeld et al., 2008). Conversely, the soil temperature in the deeper zone has maintained a relatively slight fluctuation within the range of ~2°C during the monitoring period (Text S8 in Supporting Information S1). Remarkably, the temperature response near the depth of ~20 m to rain-falls offers interesting insights into the hydromechanical behavior of the slip zone, as discussed later.

As mentioned above, the regular temperature increment data are inverted to estimate the formation's hydrogeological information. Given the difficulty in deep borehole sampling and laboratory calibration of fractured and intact sandstones, the moisture content along the whole profile in this study has been inferred based on the calibration test results of soil samples collected within 0–3 m depths (Figure S3 in Supporting Information S1). It is rational to capture subsurface fluid activity despite inevitable estimation errors (Text S9 in Supporting Information S1). As illustrated in Figure 3b, the responses of moisture variation at shallower depths are highly consistent with rainfall events, implying precipitation-infiltration recharge at the near-surface zone. This demonstrates the sensitivity and effectiveness of moisture measurement using AH-WFBG sensing. Strikingly, we discovered variations in moisture content near the depth of 20 m across the monitoring span and linked these variations to rainfall events and landslide kinematics (Zhang & Xue, 2019). A narrowband representing the lower moisture content was also observed at a depth of 29 m, which spread and thickened in mid-to-late July when it was hot and

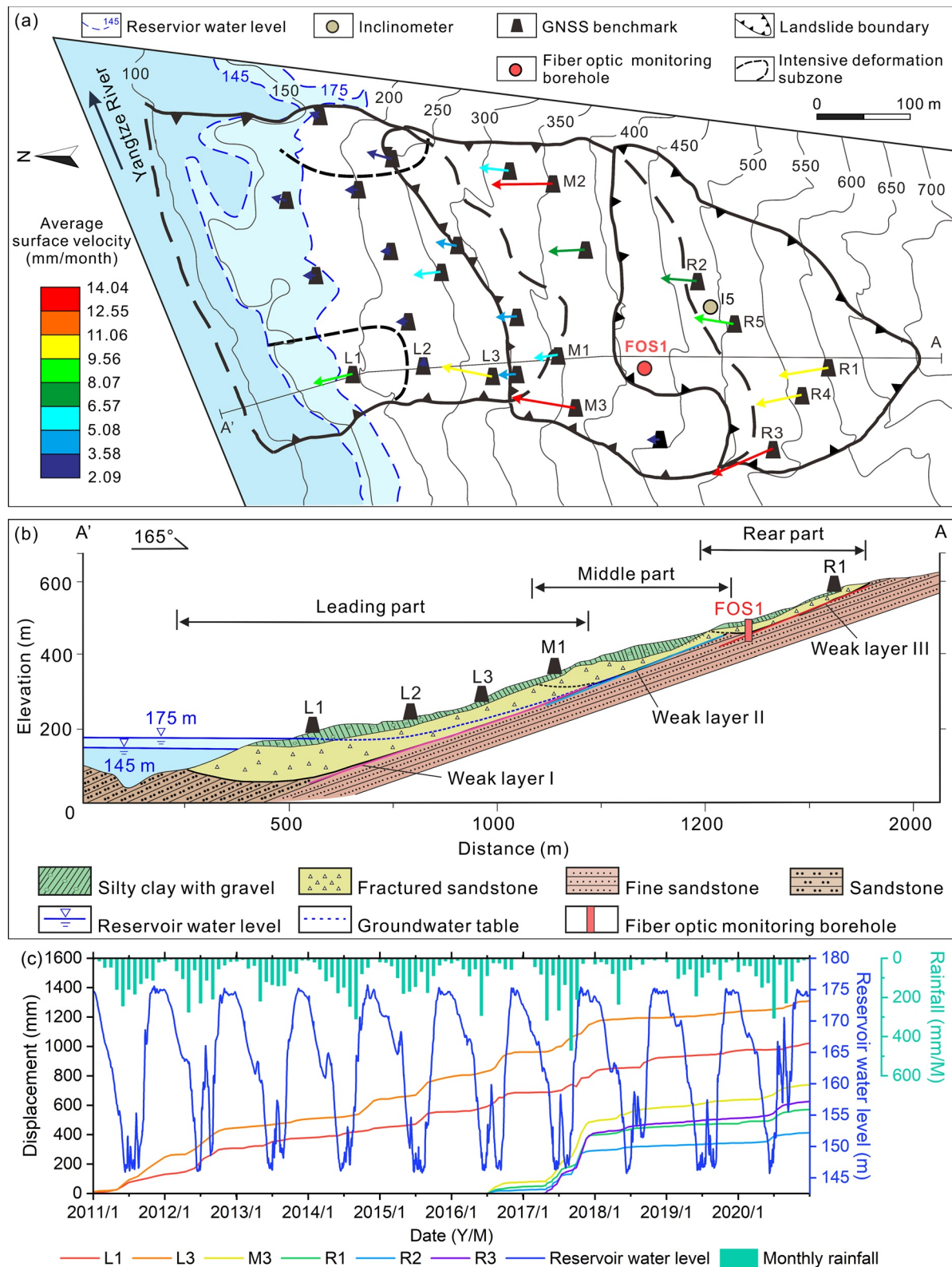


Figure 2. Geographical, geological, and historical kinematic information of the Outang landslide. (a) Plan view of the landslide with in-place instrumentation and spatial distribution of the surface displacements (vector arrows with color). (b) Geological profile of cross-section A–A'. (c) Cumulative displacements with the reservoir water levels (RWLs) and rainfalls from 2011 to 2020.

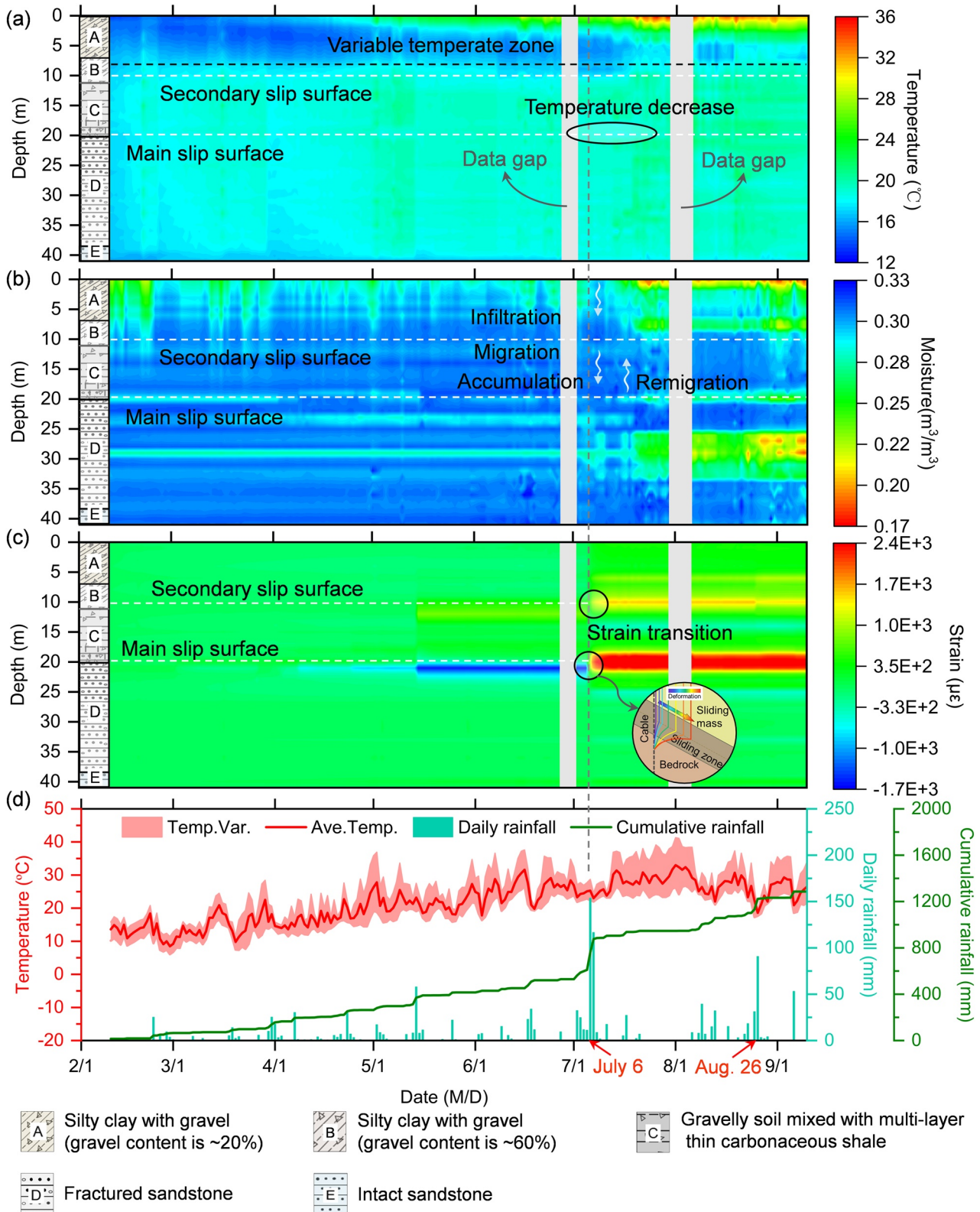


Figure 3. Spatiotemporal evolution of subsurface multi-physics of the borehole FOS1 and meteorological records. (a) Temperature. (b) Moisture. (c) Strain. The positive value represents tensile strain. (d) Atmospheric temperature records and rainfall events from February 10 to September 10, 2021.

relatively rainless. This might be explained by the impermeable filler at this depth and the existence of a relatively sound sandstone with few fractures.

Distinctive strain variations are found at depths of approximately 10 and 20 m (Figure 3c). An apparent tensile strain was witnessed at a depth of 20 m, with a peak value of 2,856 $\mu\epsilon$. Specifically, a dramatic change in strain occurred on July 6, when the daily rainfall of 153.7 mm reached a new high this year. A similar phenomenon was also observed at a depth of 10 m during the same period, with a maximum strain of 1,584 $\mu\epsilon$. The strain rate data reflecting the stress state (i.e., compressive or tensile) of the sensing cable are closely related to the landslide stability conditions (Scaringi et al., 2018). The magnitude of the peak strain rate in this study exceeded 500 $\mu\epsilon/d$ at the shallower slip surface and even more than 1,000 $\mu\epsilon/d$ at the deeper slip surface (Figure S9 in Supporting Information S1). It can be deduced that these two bands of strain accumulation were two critical slip surfaces (Kogure & Okuda, 2018; Zhang, Zhu, et al., 2018).

Altogether, these results show that the soil temperature had slightly decreased, whereas moisture content increased at a depth of 20 m when frequent rainfall events occurred (Figure 3). This has been attributed to precipitation infiltration from the surface to deep soils and water migration toward this main slip surface (mid-May to early July 2020), indicating the rise of pore water pressure at this location. Part of the overburden layers around \sim 20 m depth absorbs pore fluid derived from rainfall recharge, forming an unconfined seasonal aquifer. The shear band composed of clay-like materials could act as an impermeable barrier that accumulates migrated pore fluid, thus resulting in the significant strength degradation of the geomaterials (Seguí & Veveakis, 2021). This is the reason why the temperature of the overburden layers decreased, especially near the depth of \sim 20 m. When large shear deformation had occurred and the rainfall was less or lighter in mid-late July, the moisture in the slip zone moved backward to the adjacent layers. However, variations in temperature and moisture at the secondary slip surface (at 10 m depth) were not remarkable due to a shorter thermo-hydro transport pathway subject to meteorological impacts.

5. Identification of Driving the Accelerated Movement

To further confirm the slip surface position, we compared the results regarding deep-seated deformation at this section of the landslide. Figure 4b depicts that the nearby inclinometer has detected the slip surface at a depth of \sim 24 m (Luo & Huang, 2020), which validates the identification that the slip surface was revealed by our borehole deployment. The depth discrepancy is considered acceptable considering the complex microrelief and difference in stratigraphy. Note that the inclinometer failed to work due to the dislocation of the inclinometer casing induced by excessive shear movements in the rainy season of 2014, which was a common problem for field monitoring in this region. This, in turn, demonstrates the advantage of near-distributed strain sensing over conventional displacement measuring techniques in accurate and long-term monitoring of subsurface deformation.

Furthermore, strain measurements are utterly dependent on deformation patterns of the sliding mass (Figure 3c). Our previous studies on the kinematic method for estimating shear displacements show that the relative positions of the cable and the sliding surface determine the strain distribution mode (Zhang, Zhu, et al., 2018; Sang et al., 2019). In this study, the strain near the main slip surface at the rear slope represents a normal distribution with a peak value, consistent with the proposed kinematic model with an acute angle between the cable axis (downward) and the sliding direction (Figure S10 in Supporting Information S1). Strikingly, we also observed the evolution of another peak strain at a depth of \sim 10 m, which was inferred as the secondary slip surface newly generated and had not been revealed by the inclinometer 15. The data confirms that the deformation of this layer developed synchronously with that of the main slip surface (Figures 4a and 4d). Given that the landslide sliding zones in the TGR area feature silty clay with gravel (Wang et al., 2021; Yin et al., 2016), the material composition at this level provides another evidence on whether it is a secondary slip surface. Further tracking and multi-source sensor measurements will allow for a more comprehensive knowledge of this shallow slip surface.

To deconvolute complexity between accelerated deformation and predisposing factors for this landslide, we examined the relationship between surface/subsurface kinematics and the RWL fluctuations/rainfalls (Figures 4c–4e). Results show that the slide moved at a very slow rate before July 6, accompanied by a prolonged drawdown and slight fluctuations of the RWL (Figure 4e). This suggests that the changes in RWL have little effect on the deformation in the rear part, which is thoroughly different from the motions in the toe that are primarily driven by

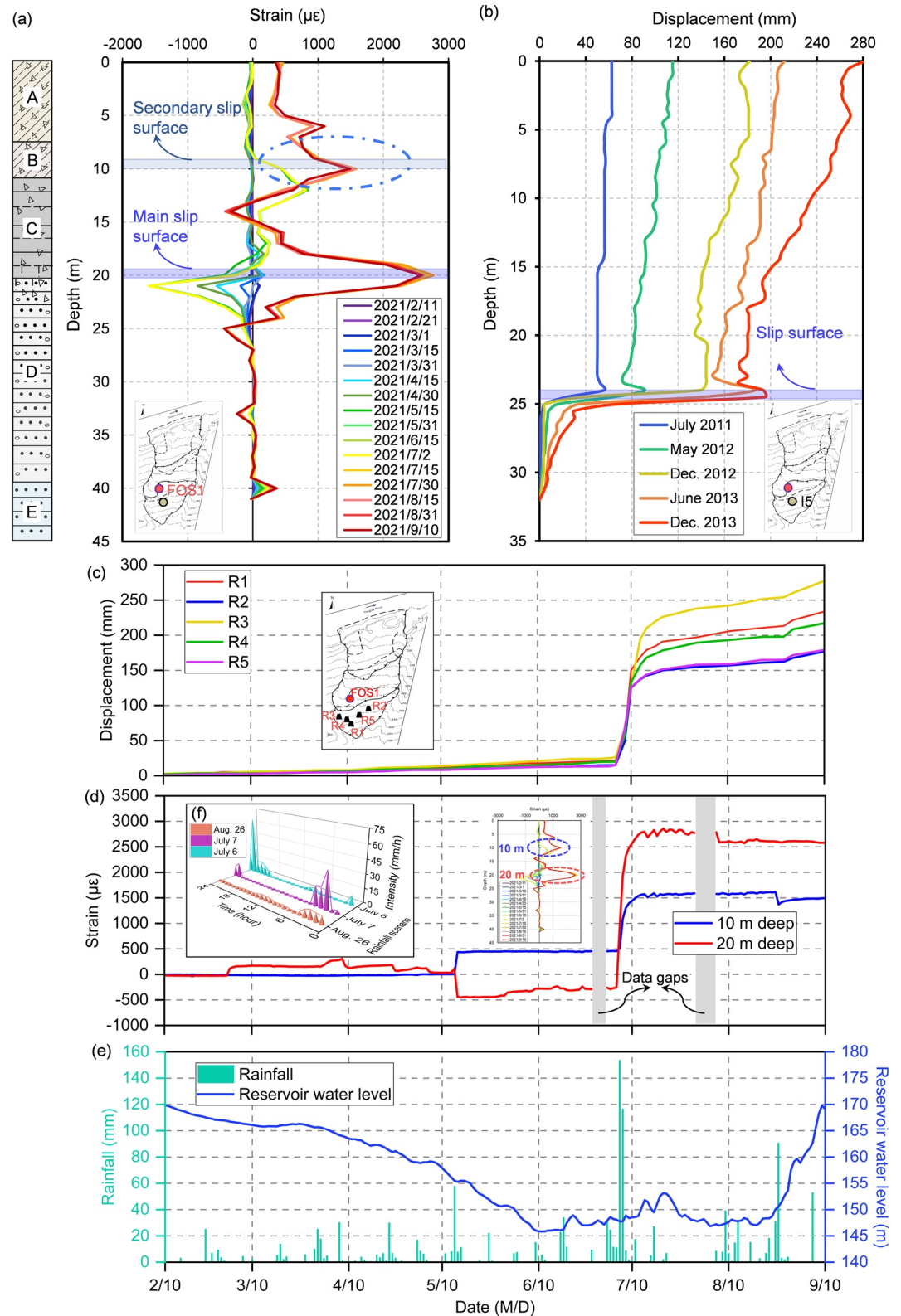


Figure 4. Surface and subsurface kinematics in the rear part of the landslide and potential drivers. (a) Strain in Borehole FOS1. (b) Displacement measured by the probe inclinometer I5 adjacent to Borehole FOS1 (adapted from Luo & Huang, 2020). (c) Surface displacement recorded by GNSS. (d) Strain of sliding surfaces. (e) Daily rainfalls and RWL fluctuations. (f) Hourly rainfall intensity of three rainstorm scenarios during the monitoring period, is inset into (d).

the reservoir scheduling (Wang et al., 2021). We noted an immediate acceleration of the surface and subsurface deformation due to the torrential rainfall on July 6. Accordingly, we conclude that the deformation in the rear slope was dominated by continuous/heavy rainfall.

To determine whether a large amount of rainfall drives accelerated movement, we considered the hourly intensity of three torrential rain events and compared their temporal characteristics, given the precipitation classification from the China Meteorological Administration (Table S4 in Supporting Information S1; Figure 4f). Results indicate that rainfalls with an extreme intensity on July 6 and 7 triggered abrupt surface and subsurface deformation. In contrast, the rainfall on August 26, representing a relatively uniform intensity, simply precipitated slight surface motions. It, therefore, seems that with similar rainfall amount and identical duration, short high-intensity storms are the main driver of deformation acceleration rather than prolonged low-intensity rainstorms (Fan et al., 2020). Yet the latter is normally considered a precursor of rainfall-induced landslides. The reason for this fascinating finding is the unique terrace landform and local agricultural activities provide a positive contribution to the infiltration and migration of rainwater to deeper layers and moisture accumulation around the slip surface. Coupled with the formation and propagation of large tension cracks in the active rear slope (Text S10 and Figure S11 in Supporting Information S1), this situation strongly favors a large amount of rainwater catchment and infiltration processes (Nereson et al., 2018; Zhang & Xue, 2019). Additionally, asymmetric distributions of peak rainfall intensities that occurred on July 6 and July 7 were superimposed (Figure 4f), thus significantly affecting the whole landslide dynamics.

6. Do We Need Near-Distributed Thermo-Hydro-Mechanical Monitoring?

Temperature is rarely used to interpret landslide stability, yet more attention should be paid to long-term monitoring of subsurface temperature (Shibasaki et al., 2016; Tang et al., 2019). Multiple pieces of evidence have suggested that evolutionary temperature is implicated in pore fluid activity in rock and soil masses, which offers a possibility to predict and assess landslide stability (Seguí et al., 2020). A major advantage of near-distributed thermo-hydro-mechanical monitoring is to accurately locate the slip surface and produce spatiotemporal profiles of temperature, moisture and strain. Intriguingly, a multi-field monitoring system can be constructed with only one homologous monitoring technology (i.e., fiber-optic), which greatly enhances the robustness and integration of the system, and avoids the dilemma of multi-source sensing data fusion (Zhu et al., 2017).

Another benefit is that these critical data allow us to learn and decipher the multi-physical evolution characteristics of reservoir landslides. The time- and depth-varying dataset can provide improved insights into the subsurface thermo-hydro-mechanical link among external conditions, hydromechanical dynamics and geotechnical deformation (Zhang & Xue, 2019), leading to a better understanding of the evolution mechanism of reservoir landslides.

Figure 1a also outlines the evolution processes of a reservoir landslide. This figure illustrates the cyclic thermo-hydro-mechanical processes within the slope, which may promote weakening and progressive failure of rock and soil masses. For a giant reservoir landslide, the periodic RWL fluctuations that accompany seasonal alternation of atmospheric temperature and precipitation are external conditions of the thermo-hydro-mechanical characteristics (Hugentobler et al., 2020). In case of rapid dropdown of the RWL, a suspended groundwater table emerges since the pore water pressure is difficult to dissipate immediately. The landslide toe then undergoes an unloading process, resulting in outward seepage force that tends to destabilize the slope. The Outang landslide is a typical giant landslide explicitly showing this seepage-driven characteristic with a dragging effect (Yin et al., 2016). Large tension cracks developed in the active rear slope further propagated and became longer, wider and deeper, which played a crucial role in providing channels for rainwater rapid infiltration and migration. This facilitated the increase of pore water pressure at slip surfaces and reduction in shear strength of the soil. This synergistic effect of dragging and pushing promotes the accelerated movement of giant reservoir landslides in the TGR area.

7. Conclusions

In this work, we describe the design, implementation, and evaluation of a fiber-optic nerve system for monitoring a reservoir landslide using weak-reflection fiber Bragg gratings. The system has been installed and operated at the active rear part of the Outang landslide in the TGR region, China. This high-resolution monitoring system enables

us to obtain a critical subsurface multi-physical dataset regarding temperature, moisture, and strain remotely and in real-time. The dataset allows us to produce the spatiotemporal evolution profiles of multi-physical information, making it possible to witness the processes of subsurface thermo-hydro-mechanical interactions and improve the understanding of the causes, triggers and mechanisms of reservoir landslides.

The measured results were encouraging for investigating how a giant reservoir landslide evolved. We have successfully confirmed the main slip surface and identified a secondary slip surface newly generated in the rear slope. The response of temperature and moisture near the main slip surface representing pore fluid migration explains the accelerated shear movement (Neresson et al., 2018; Schulz et al., 2018). We have argued that the surface and subsurface kinematics in the upper part is strictly related to large-amount rainfalls and then deciphered that short-duration high-intensity storms accounted for the abrupt motion on 6 July 2021, contradicting the expected relationship. Temporal patterns of rainfall events highlight the notable contribution of extreme precipitation to landslide triggering, and the significance of high-precision satellite precipitation products for early warning (Ravuri et al., 2021; Thomas et al., 2019). Worryingly, evidence that extreme rainfall events are increasing at a global scale has significantly strengthened in recent years (especially for sub-daily extreme rainfall), which may trigger cascading geohazards and challenge the accurate prediction and early warning of reservoir landslides (Westra et al., 2014; Hu et al., 2022; Zhang et al., 2021; Zheng et al., 2021). Thus, the combination of multidisciplinary approaches is helpful to advance the characterization and analyses of landslide dynamics (Hu et al., 2020). Frequent extreme weather events in recent years have stimulated the formation of secondary sliding surfaces in many landslides in the TGR region. The impact of unique terrace landforms and human activities in this region on geohazard evolution was previously underestimated, and some phenomena have not been explained by our current knowledge. Our data will allow us to investigate subsurface multi-physical characteristics from daily to annual scales and relate the cyclic thermo-hydro-mechanical external conditions to creeping motion and progressive failure. The system can be coupled with remote sensing and other ground-based technologies to build a space-sky-ground-subsurface integrated monitoring framework for reservoir landslides (Xu et al., 2020).

Data Availability Statement

Data to support this study are available on repository: <https://doi.org/10.5281/zenodo.6541529>.

Acknowledgments

This work was funded by the National Key Research and Development Program of China (2018YFC1505104) and the National Natural Science Foundation of China (42077235 and 41722209). Special thanks go to Hua-Fu Pei, Dalian University of Technology, Wei Zhang and Gang Cheng, Nanjing University for their contribution to the planning and installation of the monitoring system. We also thank Kun Tian for his support for geological information collection of the study area, Bing Wu and Tian-Cheng Xie for data processing, Xing Zheng and Cheng-Cheng Zhang for their kind support and suggestions in the revised version. The manuscript benefited markedly from the insightful comments and suggestions by the anonymous reviewers.

References

- AghaKouchak, A., Huning, L. S., Chiang, F., Sadegh, M., Vahedifard, F., Mazdiyasn, O., et al. (2018). How do natural hazards cascade to cause disasters? *Nature*, *561*(7724), 458–460. <https://doi.org/10.1038/d41586-018-06783-6>
- Bakker, M., Caljé, R., Schaars, F., vanderMade, K. J., & deHaas, S. (2015). An active heat tracer experiment to determine groundwater velocities using fiberoptic cables installed with direct push equipment. *Water Resources Research*, *51*, 2760–2772. <https://doi.org/10.1002/2014WR016632>
- Biggs, J., & Wright, T. J. (2020). How satellite InSAR has grown from opportunistic science to routine monitoring over the last decade. *Nature Communications*, *11*, 3863. <https://doi.org/10.1038/s41467-020-17587-6>
- Brovkin, V., Brook, E., Williams, J. W., Bathiany, S., Lenton, T. M., Barton, M., et al. (2021). Past abrupt changes, tipping points and cascading impacts in the Earth system. *Nature Geoscience*, *14*, 550–558. <https://doi.org/10.1038/s41561-021-00790-5>
- Cao, D. F., Shi, B., Loheide, S. P., II, Gong, X., Zhu, H. H., Wei, G. Q., & Yang, L. (2018). Investigation of the influence of soil moisture on thermal response tests using active distributed temperature sensing (A-DTS) technology. *Energy and Buildings*, *173*, 239–251. <https://doi.org/10.1016/j.enbuild.2018.01.022>
- Cao, D. F., Shi, B., Zhu, H. H., Wei, G. Q., Chen, S. E., & Yan, J. F. (2015). A distributed measurement method for in-situ soil moisture content by using carbon-fiber heated cable. *Journal of Rock Mechanics and Geotechnical Engineering*, *7*(6), 700–707. <https://doi.org/10.1016/j.jrmge.2015.08.003>
- Cenni, N., Fiaschi, S., & Fabris, M. (2021). Integrated use of archival aerial photogrammetry, GNSS, and InSAR data for the monitoring of the Patigno landslide (Northern Apennines, Italy). *Landslides*, *18*, 2247–2263. <https://doi.org/10.1007/s10346-021-01635-3>
- Cook, K. L., Rekapalli, R., Dietze, M., Pilz, M., Cesca, S., Rao, N. P., et al. (2021). Detection and potential early warning of catastrophic flow events with regional seismic networks. *Science*, *374*, 87–92. <https://doi.org/10.1126/science.abj1227>
- Fan, L. F., Lehmann, P., Zheng, C. M., & Or, D. (2020). Rainfall intensity temporal patterns affect shallow landslide triggering and hazard evolution. *Geophysical Research Letters*, *47*, e2019GL085994. <https://doi.org/10.1029/2019GL085994>
- Freifeld, B. M., Finsterle, S., Onstott, T. C., Toole, P., & Pratt, L. M. (2008). Ground surface temperature reconstructions: Using in situ estimates for thermal conductivity acquired with a fiber-optic distributed thermal perturbation sensor. *Geophysical Research Letters*, *35*, L14309. <https://doi.org/10.1029/2008GL034762>
- Hu, W., Li, Y., Fan, Y., Xiong, M. S., Luo, H., McSaveney, M., et al. (2022). Flow amplification from cascading landslide dam failures: Insights from flume experiments. *Engineering Geology*, *297*, 106483. <https://doi.org/10.1016/j.enggeo.2021.106483>
- Hu, X., Bürgmann, R., Schulz, W. H., & Fielding, E. J. (2020). Four-dimensional surface motions of the Slungullion landslide and quantification of hydrometeorological forcing. *Nature Communications*, *11*, 2792. <https://doi.org/10.1038/s41467-020-16617-7>
- Hu, X., Lu, Z., Pierson, T. C., Kramer, R., & George, D. L. (2018). Combining InSAR and GPS to determine transient movement and thickness of a seasonally active low-gradient translational landslide. *Geophysical Research Letters*, *45*, 1453–1462. <https://doi.org/10.1002/2017GL076623>

- Hugentobler, M., Loew, S., Aaron, J., Roques, C., & Oestreicher, N. (2020). Borehole monitoring of thermo-hydro-mechanical rock slope processes adjacent to an actively retreating glacier. *Geomorphology*, 362, 107190. <https://doi.org/10.1016/j.geomorph.2020.107190>
- Kersey, A. D., Davis, M. A., Patric, H. J., LeBlanc, M., Koo, K. P., Askins, C. G., et al. (1997). Fiber grating sensors. *Journal of Lightwave Technology*, 15, 1442–1463. <https://doi.org/10.1109/50.618377>
- Kogure, T., & Okuda, Y. (2018). Monitoring the vertical distribution of rainfall-induced strain changes in a landslide measured by distributed fiber optic sensing with Rayleigh backscattering. *Geophysical Research Letters*, 45, 4033–4040. <https://doi.org/10.1029/2018GL077607>
- Lacroix, P., Handwerger, A. L., & Bièvre, G. (2020). Life and death of slow-moving landslides. *Nature Reviews Earth & Environment*, 1(8), 404–419. <https://doi.org/10.1038/s43017-020-0072-8>
- Li, W., & Zhang, J. (2018). Distributed weak fiber Bragg grating vibration sensing system based on 3×3 fiber coupler. *Photonic Sensors*, 8(2), 146–156. <https://doi.org/10.1007/s13320-018-0410-3>
- Liu, S. P., Shi, B., Gu, K., Zhang, C. C., He, J. H., Wu, J. H., & Wei, G.-Q. (2021). Fiber-optic wireless sensor network using ultra-weak fiber Bragg gratings for vertical subsurface deformation monitoring. *Natural Hazards*, 109, 2557–2573. <https://doi.org/10.1007/s11069-021-04932-1>
- Liu, X. J., Zhao, C. Y., Zhang, Q., Lu, Z., & Li, Z. H. (2020). Deformation of the Baige landslide, Tibet, China, revealed through the integration of cross-platform ALOS/PALSAR-1 and ALOS/PALSAR-2 SAR observations. *Geophysical Research Letters*, 47, e2019GL086142. <https://doi.org/10.1029/2019GL086142>
- Luo, S. L., & Huang, D. (2020). Deformation characteristics and reactivation mechanisms of the Outang ancient landslide in the Three Gorges Reservoir, China. *Bulletin of Engineering Geology and the Environment*, 79, 3943–3958. <https://doi.org/10.1007/s10064-020-01838-3>
- Nereson, A. L., Davila Olivera, S., & Finnegan, N. J. (2018). Field and remote-sensing evidence for hydro-mechanical isolation of a long-lived earthflow in central California. *Geophysical Research Letters*, 45, 9672–9680. <https://doi.org/10.1029/2018GL079430>
- Ravuri, S., Lenc, K., Willson, M., Kangin, D., Lam, R., Mirowski, P., et al. (2021). Skilful precipitation nowcasting using deep generative models of radar. *Nature*, 597, 672–677. <https://doi.org/10.1038/s41586-021-03854-z>
- Read, T., Bour, O., Bense, V., Le Borgne, T., Goderniaux, P., Klepikova, M. V., et al. (2013). Characterizing groundwater flow and heat transport in fractured rock using fiber-optic distributed temperature sensing. *Geophysical Research Letters*, 40, 2055–2059. <https://doi.org/10.1002/grl.50397>
- Sang, H. W., Zhang, D., Gao, Y. L., Zhang, L., Wei, G. Q., Shi, B., et al. (2019). Strain distribution based geometric models for characterizing the deformation of a sliding zone. *Engineering Geology*, 263, 105300. <https://doi.org/10.1016/j.enggeo.2019.105300>
- Sayde, C., Gregory, C., Gil-Rodríguez, M., Tuffillaro, N., Tyler, S., van de Giesen, N., et al. (2010). Feasibility of soil moisture monitoring with heated fiber optics. *Water Resources Research*, 46, W06201. <https://doi.org/10.1029/2009WR007846>
- Scaringi, G., Hu, W., Xu, Q., & Huang, R. Q. (2018). Shear-rate-dependent behavior of clayey bimaterial interfaces at landslide stress levels. *Geophysical Research Letters*, 45, 766–777. <https://doi.org/10.1002/2017GL076214>
- Schulz, W. H., Smith, J. B., Wang, G. H., Jiang, Y., & Roering, J. J. (2018). Clayey landslide initiation and acceleration strongly modulated by soil swelling. *Geophysical Research Letters*, 45, 1888–1896. <https://doi.org/10.1002/2017GL076807>
- Seguí, C., Ratte, H., & Veveakis, M. (2020). On the stability of deep-seated landslides. The cases of Vaiont (Italy) and shuping (Three Gorges Dam, China). *Journal of Geophysical Research: Earth Surface*, 125, e2019JF005203. <https://doi.org/10.1029/2019JF005203>
- Seguí, C., & Veveakis, M. (2021). Continuous assessment of landslides by measuring their basal temperature. *Landslides*, 18, 3953–3961. <https://doi.org/10.1007/s10346-021-01762-x>
- Shi, B., Zhang, D., & Zhu, H. H. (2019). *Distributed fiber optic sensing for geoenvironmental monitoring* (pp. 106–115). Science Press. (in Chinese).
- Shi, B., Zhang, D., Zhu, H. H., Zhang, C. C., Gu, K., Sang, H. W., et al. (2021). DFOS applications to geo-engineering monitoring. *Photonic Sensors*, 11, 158–186. <https://doi.org/10.1007/s13320-021-0620-y>
- Shibasaki, T., Matsuura, S., & Okamoto, T. (2016). Experimental evidence for shallow, slow-moving landslides activated by a decrease in ground temperature. *Geophysical Research Letters*, 43, 6975–6984. <https://doi.org/10.1002/2016GL069604>
- Strozzi, T., Delaloye, R., Käab, A., Ambrosi, C., Perruchoud, E., & Wegmüller, U. (2010). Combined observations of rock mass movements using satellite SAR interferometry, differential GPS, airborne digital photogrammetry, and airborne photography interpretation. *Journal of Geophysical Research*, 115, F01014. <https://doi.org/10.1029/2009JF001311>
- Sun, Y. J., Zhang, D., Shi, B., Tong, H. J., Wei, G. Q., & Wang, X. (2014). Distributed acquisition, characterization and process analysis of multi-field information in slopes. *Engineering Geology*, 182, 49–62. <https://doi.org/10.1016/j.enggeo.2014.08.025>
- Tang, H. M., Wasowski, J., & Juang, C. H. (2019). Geohazards in the Three Gorges Reservoir area, China – Lessons learned from decades of research. *Engineering Geology*, 261, 105267. <https://doi.org/10.1016/j.enggeo.2019.105267>
- Thomas, M. A., Collins, B. D., & Mirus, B. B. (2019). Assessing the feasibility of satellite-based thresholds for hydrologically driven landsliding. *Water Resources Research*, 55, 9006–9023. <https://doi.org/10.1029/2019WR025577>
- Wang, J. G., Schweizer, D., Liu, Q. B., Su, A. J., Hu, X. L., & Blum, P. (2021). Three-dimensional landslide evolution model at the Yangtze River. *Engineering Geology*, 292, 106275. <https://doi.org/10.1016/j.enggeo.2021.106275>
- Wasko, C., Sharma, A., & Johnson, F. (2015). Does storm duration modulate the extreme precipitation-temperature scaling relationship? *Geophysical Research Letters*, 42, 8783–8790. <https://doi.org/10.1002/2015GL066274>
- Wei, K., Ouyang, C. J., Duan, H. T., Li, Y. L., Chen, M. X., Ma, J., et al. (2020). Reflections on the catastrophic 2020 Yangtze River basin flooding in southern China. *The Innovation*, 1(2), 100038. <https://doi.org/10.1016/j.xinn.2020.100038>
- Westra, S., Fowler, H. J., Evans, J. P., Alexander, L. V., Berg, P., Johnson, F., et al. (2014). Future changes to the intensity and frequency of short-duration extreme rainfall. *Reviews of Geophysics*, 52, 522–555. <https://doi.org/10.1002/2014RG000464>
- Xu, Q., Peng, D. L., Zhang, S., Zhu, X., He, C. Y., Qi, X., et al. (2020). Successful implementations of a real-time and intelligent early warning system for loess landslides on the Heifangtai terrace, China. *Engineering Geology*, 278, 105817. <https://doi.org/10.1016/j.enggeo.2020.105817>
- Yin, Y. P., Huang, B. L., Wang, W. P., Wei, Y. J., Ma, X. H., Ma, F., & Zhao, C. (2016). Reservoir-induced landslides and risk control in three Gorges Project on Yangtze River, China. *Journal of Rock Mechanics and Geotechnical Engineering*, 8, 577–595. <https://doi.org/10.1016/j.jrmge.2016.08.001>
- Zeni, L., Picarelli, L., Avolio, B., Coscetta, A., Papa, R., Zeni, G., et al. (2015). Brillouin optical time-domain analysis for geotechnical monitoring. *Journal of Rock Mechanics and Geotechnical Engineering*, 7(4), 458–462. <https://doi.org/10.1016/j.jrmge.2015.01.008>
- Zhang, C. C., Shi, B., Gu, K., Liu, S. P., Wu, J. H., Zhang, S., et al. (2018). Vertically distributed sensing of deformation using fiber optic sensing. *Geophysical Research Letters*, 45(11), 158–186. <https://doi.org/10.1029/2018GL080428>
- Zhang, C. C., Zhu, H. H., Liu, S. P., Shi, B., & Zhang, D. (2018). A kinematic method for calculating shear displacements of landslides using distributed fiber optic strain measurements. *Engineering Geology*, 234, 83–96. <https://doi.org/10.1016/j.enggeo.2018.01.002>
- Zhang, W. X., Furtado, K., Wu, P. L., Zhou, T. J., Chadwick, R., Marzin, C., et al. (2021). Increasing precipitation variability on daily-to-multiyear time scales in a warmer world. *Science Advances*, 7, eabf8021. <https://doi.org/10.1126/sciadv.abf8021>

- Zhang, Y., & Xue, Z. Q. (2019). Deformation-based monitoring of water migration in rocks using distributed fiber optic strain sensing: A laboratory study. *Water Resources Research*, *55*, 8368–8383. <https://doi.org/10.1029/2019WR024795>
- Zheng, Y. X., Li, S. L., & Ullah, K. (2021). Increased occurrence and intensity of consecutive rainfall events in the China's Three Gorges Reservoir area under global warming. *Earth and Space Science*, *7*, e2020EA001188. <https://doi.org/10.1029/2020EA001188>
- Zhu, H. H., Shi, B., & Zhang, C. C. (2017). FBG-based monitoring of geohazards: Current status and trends. *Sensors*, *17*(3), 452. <https://doi.org/10.3390/s17030452>